Three-Dimensional Structures of the Amyloid β Peptide (25−35) in Membrane-Mimicking Environment‡

Toshiyuki Kohno,*,§ Kuniko Kobayashi,§ Tadakazu Maeda,§,|| Kazuki Sato,§ and Akihiko Takashima§

Mitsubishi Kasei Institute of Life Sciences, Minamiooya, Machida-shi, Tokyo 194, Japan, and Department of Physics, Kitasato University, Kitasato, Sagamihara-shi, Kanagawa 228, Japan

Received July 2, 1996; Revised Manuscript Received September 17, 1996⊗

ABSTRACT: The three-dimensional structure of amyloid β peptide (25−35), which has neurotoxic activity, in lithium dodecyl sulfate micelles was determined by two-dimensional ^{1}H NMR spectroscopy with simulated annealing calculations. A total of 20 converged amyloid β peptide structures were obtained on the basis of 110 experimental constraints, including 106 distance constraints reduced from the nuclear Overhauser effect (NOE) connectivities and four torsion angle (ϕ) constraints. The atomic root mean square difference about averaged coordinates is 1.04 ± 0.25 Å for the backbone atoms (N, C$^\alpha$, C) and 1.39 ± 0.27 Å for all heavy atoms of the entire peptide. The molecular structure of amyloid β peptide in membrane-mimicking environment is composed of a short α helix in the C terminal position. The three residues from the N-terminus are disordered, but the remaining eight C-terminal residues are well-ordered, which is supported by the RMSD values of the C-terminal region, Lys^{28}-Leu^{34}. In this region, the RMS differences from averaged coordinates are 0.26 ± 0.11 Å for the backbone atoms (N, C$^\alpha$, C) and 0.77 ± 0.21 Å for all heavy atoms, which is very low compared with those for the entire peptide. The four amino acid residues from the N-terminus are hydrophilic and the other seven amino acid residues in C-terminus are hydrophobic. So, our results show that the C-terminal region of amyloid β peptide (25−35) is buried in the membrane and assumes α-helical structure, whereas the N-terminal region is exposed to the solvent with a flexible structure. This structure is very similar to membrane-mediated structure of substance P previously reported. The three-dimensional structure of a non-neurotoxic mutant of amyloid β peptide (25−35), where Asn^{27} is replaced by Ala, in lithium dodecyl sulfate micelles was also determined. The structure is similar to that of the wild type amyloid β peptide (25−35) in the C-terminal region, but the N-terminal flexible region is different. The structural comparison of amyloid β peptide (25−35), its non-neurotoxic mutant and substance P gives a structural basis to understand the mechanism of neurotoxicity caused by amyloid β peptide.

Pathological changes of Alzheimer's disease (AD) are characterized by cerebral cortical atrophy as a result of degeneration and loss of neurons. Typical histological lesions include numerous senile plaques composed of deposits of amyloid β-protein (Aβ) and neurofibrillary tangles consisting predominantly of ubiquitin and highly phosphorylated tau proteins. According to the amyloid hypothesis for the pathogenesis of AD (Hardy & Higgins, 1992), Aβ directly affects neurons, leading to neurodegeneration and formation of PHF in NFT. Consistent with this idea, primary cultures of embryonic rat hippocampal neurons undergo progressive degeneration as well as expression of an epitope for phosphorylated tau after exposure to Aβ (1−40) or its fragment peptide Aβ (25−35) (Mattson et al., 1992; Takashima et al., 1993; Yankner et al., 1990), suggesting that Aβ might play a central role in the pathogenesis of AD.

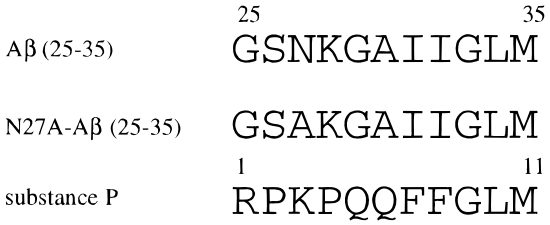

FIGURE 1: Amino acid sequences of Aβ (25−35) (A), N27A-Aβ (25−35) (B), and substance P (C).

Aβ is a 39−43 residue peptide produced by proteolytic cleavage of membrane-associated amyloid precursor protein (APP). Aβ spontaneously aggregates into amyloid fibrils *in vitro* (Kirschner et al., 1987), and is toxic to cultured cortical cells (Busciglio et al., 1993; Koh et al., 1990; Mattson et al., 1992; Yankner et al., 1990). It has been suggested that toxicity is correlated with the degree of peptide aggregation (Mattson et al., 1993; Pike et al., 1993; Tomiyama et al., 1994). An active fragment of Aβ is Aβ (25−35) having an amino acid sequence of Gly^{25}-Ser-Asn-Lys-Gly-Ala-Ile-Ile-Gly-Leu-Met^{35} (Figure 1) (Mattson et al., 1992; Pike et al., 1993; Yankner et al., 1990).

‡ Atomic coordinates for the 20 converged structures of amyloid β peptide (25−35) have been deposited with Protein Data Bank, Brookhaven National Laboratories, Long Island, NY 11973, under the accession code 1QCM.

* To whom correspondence should be addressed. FAX: +81(427)-24-6317. E-mail: tkohno@libra.ls.m-kagaku.co.jp.

§ Mitsubishi Kasei Institute of Life Sciences.

|| Kitasato University.

⊗ Abstract published in *Advance ACS Abstracts,* November 15, 1996.

[1] Abbreviations: AD, Alzheimer's disease; Aβ, amyloid β peptide; NMR, nuclear magnetic resonance; CD, circular dichroism; COSY, correlation spectroscopy; DQF-COSY, double quantum-filtered COSY; TOCSY, total correlated spectroscopy; DSS, 2,2-dimethyl-2-silapentane-5-sulfonic acid; HSQC, heteronuclear single-quantum coherence; IR, infrared spectroscopy; NOESY, nuclear Overhauser effect spectroscopy; RMSD, root mean square deviation; SDS, sodium dodecyl sulfate; LiDS, lithium dodecyl sulfate; TFE, trifluoroethanol; WATERGATE, water suppression by gradient-tailored excitation. Standard abbreviations are used for usual amino acids.

S0006-2960(96)01598-X CCC: $12.00

In order to clarify the structure-neurotoxicity relationships of the fragment, we have analyzed its neurotoxicity by using mutants in which each amino acid is replaced by Ala (Sato et al., 1995). We found that the N27A mutant where Asn^{27} is replaced by Ala [N27A-Aβ (25−35)] (Figure 1) shows lower neurotoxicity than the wild type despite its increased hydrophobicity.

Aβ has been reported to form voltage-dependent ion channels (Arispe et al., 1993a,b; Furukawa et al., 1994), and theoritical models of the possible ion channel structure have been proposed (Durell et al., 1994). It has also been reported to interact with substance P receptor (Shimohigashi et al., 1993; Yankner et al., 1990) and serpin−enzyme complex receptor (Boland et al., 1995). These studies suggest that the membrane-bound form of Aβ is important for neurotoxic activity. In order to clarify the structure−function relationships of Aβ, it is essential to determine the membrane-mediated structure of Aβ and compare it with that of non-neurotoxic mutants.

In the present study, we have analyzed the three-dimensional structures of Aβ (25−35) and N27A-Aβ (25−35) in a membrane-mimicking environment using NMR and compared the structures with each other. The relationship between structure and function of Aβ will be discussed.

MATERIALS AND METHODS

Materials. Amyloid β peptides were chemically synthesized in a large quantity by the same strategy as described previously (Sato et al., 1995). The primary structure and purity of the synthetic peptide were confirmed by analytical HPLC, amino acid analysis, and FAB-MS measurement. Deuterated sodium dodecyl sulfate (SDS-d_{25})was purchased from ISOTEC Inc. Deuterated lithium dodecyl sulfate (LiDS-d_{25}) was prepared by exchanging the sodium ion of the deuterated sodium dodecyl sulfate by using Dowex 50W×8 (Bio-Rad) cation exchanger in a lithium ion form.

NMR Spectroscopy. The samples for NMR experiments were prepared at a concentration of approximately 2 mM of Aβ (25−35) or N27A-Aβ (25−35) in either 99.96% ^2H_2O or 90% H_2O/10% ^2H_2O containing 250 mM LiDS-d_{25} at pH 4.0. Under these conditions, the NMR spectra are well resolved and no aggregation can be observed over a period of several months. NMR measurements were performed using standard pulse sequences and phase cycling on a Bruker AMX-500 spectrometer operating at 500 MHz for the proton frequency. All two-dimensional NMR spectra were acquired in a phase-sensitive mode using the time-proportional phase incrementation (Marion & Wüthrich, 1983) for quadrature detection in the t_1 dimension. NOESY spectra (Jeener et al., 1979; Macura et al., 1981) were recorded at temperatures of 35 and 45 °C with mixing times of 75, 150, and 300 ms, respectively. TOCSY spectra were recorded using a MLEV-17 pulse scheme (Bax & Davis, 1985) with isotropic mixing times of 50 and 80 ms. The suppression of the solvent resonance was achieved by using the WATERGATE scheme in both NOESY and TOCSY spectra (Piotto et al., 1992). A DQF-COSY (Rance et al., 1983) spectrum was recorded to obtain the constraints for torsion angles. The suppression of the solvent resonance was achieved by using coherence selection with a gradient-enhanced method (Hurd, 1990; von Kienlin et al., 1991). No selective irradiation during the relaxation delay period was used to suppress the solvent resonance. A $^1H-^{13}C$ HSQC spectrum was recorded to obtain the chemical shifts of α carbon resonances. The suppression of the solvent resonance was achieved by using the WATERGATE scheme (Sklenár et al., 1993). Data size for HSQC spectrum was 512 (t_1) × 2048 (t_2) and spectral widths were 12 kHz in the ^{13}C dimension and 5000 Hz in the ^1H dimension.

Data processing was performed either on a Bruker X-32 UNIX workstation with UXNMR software or on a Kubota Titan 750V with NMRZ software (New Methods Research Inc.). Phase-shifted sine-squared window functions were applied prior to Fourier transformation, with shifts of $\pi/3$ to $\pi/2$ in both dimensions. Final matrix sizes were usually 2048 × 2048 real points.

Chemical shifts were referenced to the methyl resonance of 2,2-dimethyl-2-silapentane-5-sulfonic acid (DSS) used as an internal standard. Complete sets of the two-dimensional spectra were recorded at 35 °C and pH 4.0 (uncorrected meter readings).

Distance Constraints and Structure Calculations. Inter-proton distance restraints were obtained from the NOESY spectra with mixing times of 75, 150, or 300 ms. Quantitative determination of cross-peak intensities was based on the counting of the contour levels. All NOE data were divided into three classes, strong, medium, and weak, corresponding to distance upper limits of 2.5, 3.5, and 5.0 Å in the inter-proton distance restraints. Pseudo-atoms were used for non-stereospecifically assigned protons, and intra-residue and long-range correcting factors were added to the distance restraints, respectively (Wüthrich et al., 1983). In addition, 0.5 Å was added to the upper limits for distance restraints involving methyl protons (Clore et al., 1987).

All calculations were carried out on an HP 9000/720 workstation with the X-PLOR 3.1 program (Brünger, 1993). The three-dimensional structures were calculated on the basis of the experimentally derived distance and torsion angle constraints using a dynamically simulated annealing protocol starting from a template structure with randomized backbone ϕ and ψ torsion angles.

Evaluation Methods. The convergence of the calculated structures was evaluated in terms of the structural parameters, i.e., RMS deviations from experimental distance and dihedral constraints, the values of energetic statistics (F_{NOE}, F_{tor}, and F_{repel}), and RMS deviations from idealized geometry. The distribution of backbone dihedral angles of the final converged structures were evaluated by the representation of the Ramachandran dihedral pattern, indicating the deviations from the sterically allowed (ϕ, ψ) angle limits (Ramachandran et al., 1963). The degree of angular variation among the converged structures were further assessed by using an angular order parameter S (Davis et al., 1993; Hyberts et al., 1992). The order parameter S was calculated by using the following equation.

$$S = \frac{1}{N}[(\sum_{j=1}^{N} \sin\theta_j)^2 + (\sum_{j=1}^{N} \cos\theta_j)^2]^{1/2}$$

N is the number of total converged structures. θ_j is a particular dihedral angle of the jth structure of the total structures.

Temperature Coefficients and NH-Hydrogen Exchange. Temperature coefficients ($-\Delta\delta/\Delta T$, ppb) were obtained using

data from TOCSY spectra acquired at 15.0, 20.0, 25.0, 30.0, and 35.0 °C and were calculated from plots of chemical shift versus temperature which were linear for all amide protons in both Aβ (25−35) and N27A-Aβ (25−35). For slowly exchanging backbone amide protons, the sample lyophilized from H_2O was redissolved in ^2H_2O and identified by analysis of TOCSY spectra recorded at time scales of 0.5, 2.0, 3.5, 5.0, 6.5, and 8.0 h. A complete set of the two-dimensional spectra was recorded at 15 °C.

RESULTS

Sequential Resonance Assignments and Chemical Shifts. Sequence-specific resonance assignments were made according to the standard method established by Wüthrich and co-workers (1986). The proton resonances of both Aβ (25−35) and N27A-Aβ (25−35) were assigned to the spin systems of specific amino acid types by analyzing scalar coupling patterns observed in DQF-COSY and TOCSY spectra. The identified spin systems were then aligned along the primary structure of the molecule through inter-residue sequential NOEs observed on the NOESY spectra. Inter-residue sequential connectivities were carried out by analysis of the $C^{\alpha}H(i)-NH(i+1)$ ($d_{\alpha N}$), $NH(i)-NH(i+1)$ (d_{NN}), and $C^{\beta}H(i)-NH(i+1)$ ($d_{\beta N}$) NOEs.

Since Ser, Asn, Lys, Ala, Leu, and Met are present only once in the primary sequence of Aβ (25−35), these residues were used as starting points for the sequential assignment process. In particular, the assignment of Ser[26], Lys[28], Ala[30], and Met[35] resonances were straightforward. The spin system for Ala[30] residue was assigned through the observation of strong cross-peaks between methyl protons and $C^{\alpha}H$ in the DQF-COSY spectrum and the magnetization transfer from $C^{\alpha}H$ to $C^{\beta}H_3$ in the TOCSY spectrum. The assignment of resonances of N27A-Aβ (25−35) was assisted by the assignment of Aβ (25−35).

Figure 2A and 2B show the $C^{\alpha}H$-NH fingerprint region of the NOESY spectrum containing sequential $d_{\alpha N}(i, i+1)$ connectivities of Aβ (25−35) and N27A-Aβ (25−35), respectively. The complete sequence-specific resonance assignments of both Aβ (25−35) and N27A-Aβ (25−35) summarized in Table 1. Figure 3 represents sequential NOE connectivities observed in the 300 ms NOESY spectrum.

The proton chemical shifts of each residue of Aβ (25−35) and N27A-Aβ (25−35) is similar to each other, especially, in the C-terminal portion of Gly[29]-Met[35]. The differences in the portion between two peptides are almost negligible (Table 1), which suggest the structural similarity in this portion. In the N-terminal region, however, there are small differences of the proton chemical shifts. For example, the differences of the chemical shifts of $C^{\alpha}H$ of Ser[26] and Lys[28] are larger than 0.08 ppm between Aβ (25−35) and N27A-Aβ (25−35), which suggest the structural differences in the N-terminal region.

Dihedral Angles. The backbone $NH-C^{\alpha}H$ coupling constants were estimated on the DQF-COSY spectrum and were converted to backbone torsion angle ϕ constraints according to the following rules: $^3J_{NH-C^{\alpha}H}$ less than 5.5 Hz constrained the ϕ angle to the range of $-65 \pm 25°$, and $^3J_{NH-C^{\alpha}H}$ greater than 8.0 Hz constrained to the range of $-120 \pm 40°$ (Pardi et al., 1984). In the case of Aβ (25−35), four residues (Lys[28], Ala[30], Ile[31], and Ile[32]) with $^3J_{NH-C^{\alpha}H}$ less than 5.5 Hz and the other residues except for Gly[29] and Gly[33] with $^3J_{NH-C^{\alpha}H}$ between 5.5 and 8.0 Hz, a total of four backbone torsion ϕ angles were constrained. In the case of N27A-Aβ (25−35), four residues (Ala[27], Lys[28], Ala[30], and Ile[31]) with $^3J_{NH-C^{\alpha}H}$ less than 5.5 Hz and the other residues except for Gly[29] and Gly[33] with $^3J_{NH-C^{\alpha}H}$ between 5.5 and 8.0 Hz, a total of four backbone torsion ϕ angles were constrained. For both peptides, residues 29 and 33 are glycines. Therefore $^3J_{NH-C^{\alpha}H}$ values for these residues were not determined.

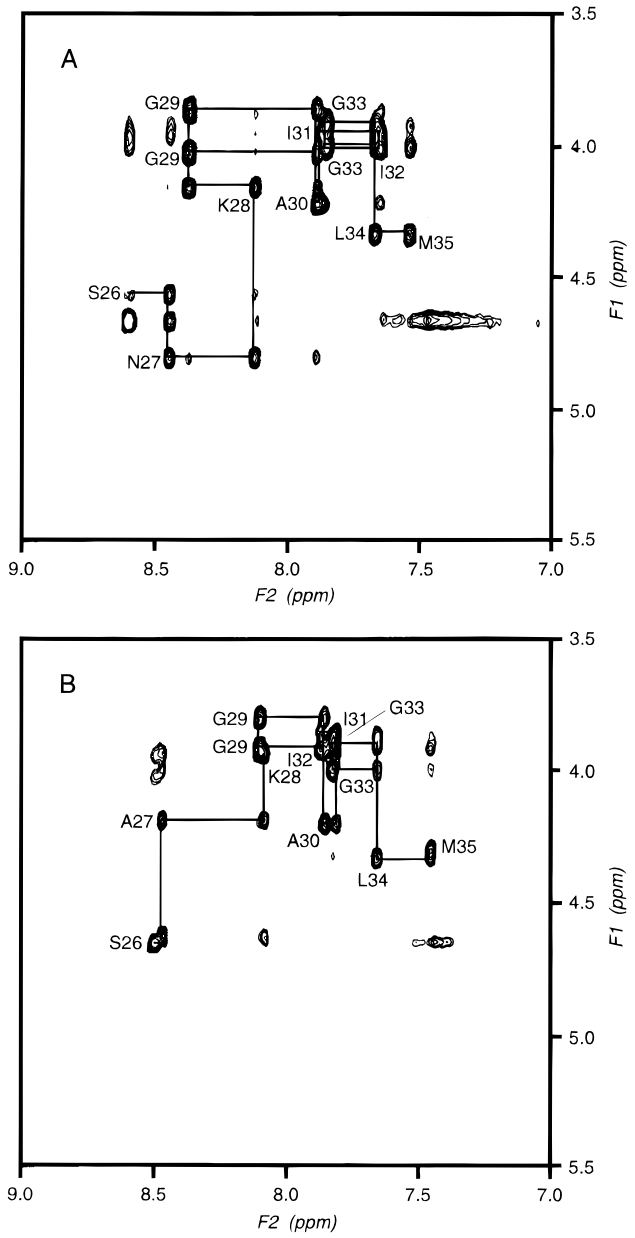

FIGURE 2: Portions of the 500 MHz two-dimensional NMR spectra of 2.0 mM Aβ (25−35) and N27A-Aβ (25−35) in 250 mM of LiDS-d_{25} and 90% H_2O/10% ^2H_2O at pH 4.0 and 35 °C. Sequential $d_{\alpha N}(i,i+1)$ NOE connectivities for residues from 25 to 35 in the NOESY spectrum observed with a mixing time of 300 ms of Aβ (25−35) (A) and N27A-Aβ (25−35) (B). In the spectral portions, the intra-residue NH-$C^{\alpha}H$ cross-peaks are labeled with the residue number by standard single-letter amino acid abbreviations.

Secondary Structure. The regular secondary structure elements of Aβ (25−35) and of N27A-Aβ (25−35) were identified according to standard criteria (Wüthrich et al., 1984). The extents of α-helices were based on small $^3J_{NH-C^{\alpha}H}$ coupling constants, strong sequential d_{NN}, strong $d_{\alpha\beta}(i,i+3)$. The representation of the $C^{\alpha}H$ or C^{α} chemical

Table 1: Chemical Shifts (in ppm) of ^{1}H Resonances of Aβ at 35 °C and pH 4.0[a]

residue	NH	C$^\alpha$H	C$^\beta$H	others
		(A) Aβ (25−35)		
Gly25	*b*	*b*		
Ser26	8.59	4.55	3.89, 3.94	
Asn27	8.45	4.80	2.84, 2.84	N$^\delta$H 6.85, 7.47
Lys28	8.12	4.15	1.85, 1.85	C$^\gamma$H 1.43, 1.50; C$^\delta$H 1.71, 1.71; C$^\epsilon$H 3.03, 3.03
Gly29	8.37	3.84, 4.02		
Ala30	7.88	4.21	1.48	
Ile31	7.86	3.94	2.03	C$^\gamma$H$_3$ 0.94; C$^\gamma$H 1.26, 1.60; C$^\delta$H 0.90
Ile32	7.64	4.00	1.94	C$^\gamma$H$_3$ 0.97; C$^\gamma$H 1.29, 1.56; C$^\delta$H 0.91
Gly33	7.85	3.89, 3.99		
Leu34	7.66	4.33	1.82, 1.82	C$^\gamma$H 1.62; C$^\delta$H 0.88, 0.94
Met35	7.53	4.33	2.07, 2.15	C$^\gamma$H 2.53, 2.62
		(B) N27A-Aβ (25−35)		
Gly25	*b*	*b*		
Ser26	8.51	4.64	3.95, 4.02	
Ala27	8.49	4.21	1.49	
Lys28	8.10	3.97	1.84, 1.84	C$^\gamma$H 1.43, 1.51; C$^\delta$H 1.75, 1.75; C$^\epsilon$H 3.00, 3.00
Gly29	8.12	3.83, 3.92		
Ala30	7.88	4.23	1.52	
Ile31	7.83	3.89	2.01	C$^\gamma$H$_3$ 0.94; C$^\gamma$H 1.25, 1.70; C$^\delta$H 0.87
Ile32	7.89	3.95	1.96	C$^\gamma$H$_3$ 0.98; C$^\gamma$H 1.34, 1.62; C$^\delta$H 0.90
Gly33	7.86	3.91, 4.02		
Leu34	7.68	4.36	1.90, 1.90	C$^\gamma$H 1.64; C$^\delta$H 0.92, 0.96
Met35	7.48	4.31	2.08, 2.17	C$^\gamma$H 2.54, 2.67

[a] The ^{1}H chemical shifts are referenced to internal 2,2-dimethyl-2-silapentane-5-sulfonic acid (DSS). [b] Not detected.

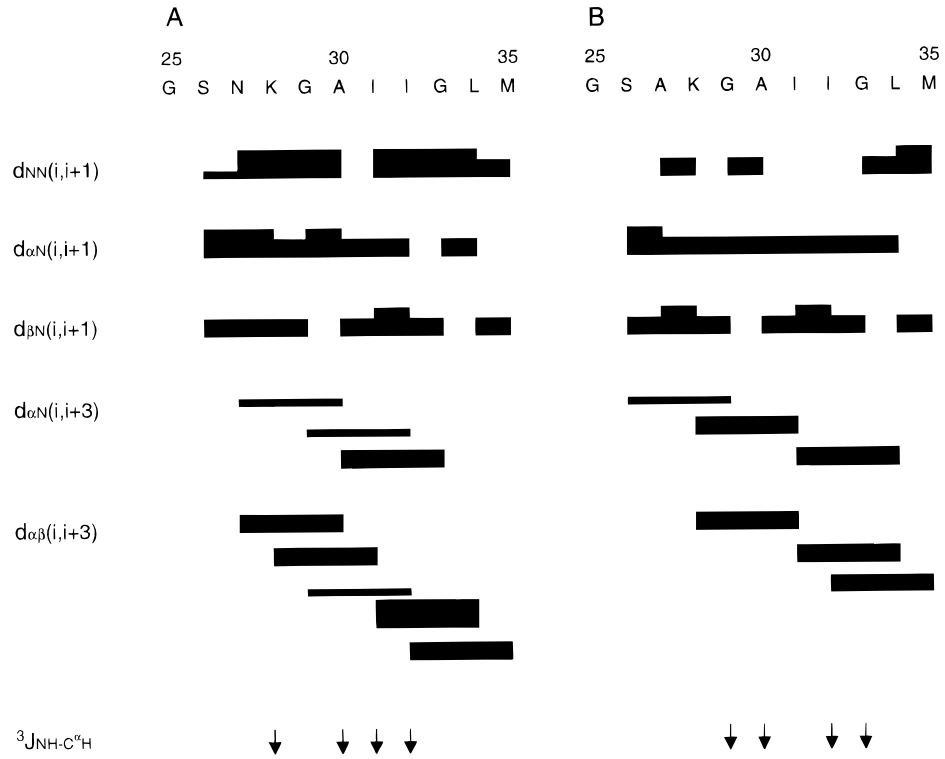

FIGURE 3: Summary of the NOE connectivities and $^3J_{NH-C^\alpha H}$ coupling constants observed in Aβ (25−35) (A) and N27A-Aβ (25−35) (B). These structural parameters were used for the sequence-specific assignments and the identification of secondary structure elements in both Aβ (25−35) and N27A-Aβ (25−35). The NOEs, d_{NN}, $d_{\alpha N}$, and $d_{\beta N}$ are indicated by bars between two residues. The NOEs are classified into strong, medium and weak according to the height of the filled bars. Values of $^3J_{NH-C^\alpha H}$ coupling constants are indicated by ↓ (<5.5 Hz) symbols. As for residues 25 and 33, $^3J_{NH-C^\alpha H}$ were not determined because they are glycine residues.

shift also served as a good indicator, identifying the presence or location of secondary protein structure by using the comparative deviation of the chemical shifts of C$^\alpha$H or C$^\alpha$ from those in random-coil structure (Spera & Bax, 1991; Wishart et al., 1992). On the basis of the results summarized in Figure 4, both Aβ (25−35) and N27A-Aβ (25−35) consist mainly of α-helices at least in the middle of the sequence.

Structure Calculations and Evaluation. To determine the three-dimensional structures of Aβ (25−35) and N27A-Aβ (25−35) in solution, we carried out the structural calculation using an X-PLOR simulated annealing protocol. In the case of Aβ (25−35), the input data of the NMR experimental constraints consisted of 106 distance and four dihedral constraints. All 106 distance constraints include 48 intra-

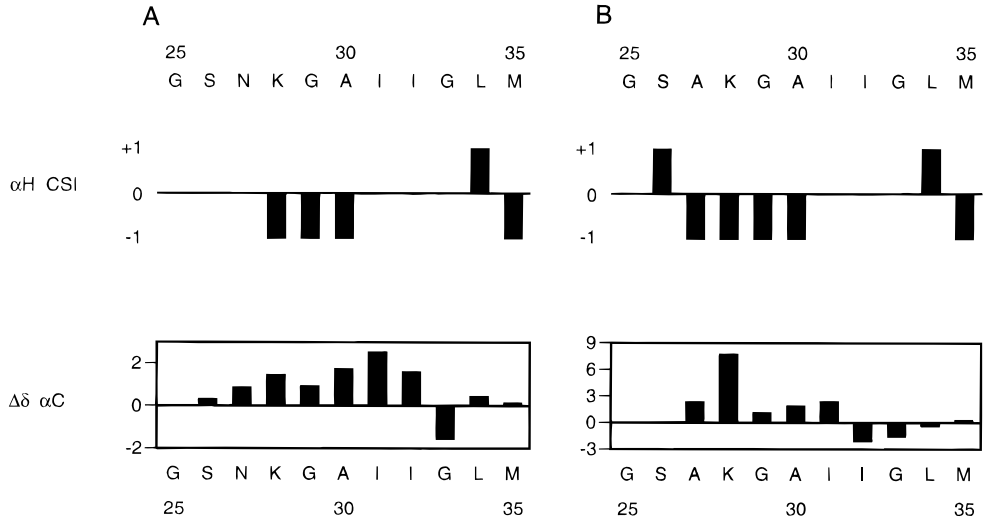

FIGURE 4: Chemical shift indices of the $C^{\alpha}H$ resonances and deviation of $^{13}C^{\alpha}$ resonances from random coils for Aβ (25−35) (A) and N27A-Aβ (25−35) (B). The chemical shift indices of the $C^{\alpha}H$ resonances are indicated by ternary indices with values of −1, 0, and 1. The values of −1 and 1 indicate a shift deviation from the random-coil value of greater than 0.1 ppm upfield and downfield, respectively, whereas those within the range of random-coil value are indicated by 0 (Wishart & Sykes, 1994; Wishart et al., 1992).

Table 2: Structural Statistics for Aβ (25−35) and N27A-Aβ (25−35)[a]

structural parameter	converged structures	mean structure
Aβ (25−35)	20 converged	
RMS deviations from experimental distance constraints (Å)		
all (106)	0.063 ± 0.005	0.058
intraresidue (48)	0.080 ± 0.008	0.074
sequential (35)	0.047 ± 0.008	0.042
medium-range ($\|i - j\| < 5$) (23)	0.036 ± 0.007	0.035
RMS deviation from experimental dihedral constraints (deg) (4)	0.062 ± 0.226	0.0
energetic statistics (kcal mol^{-1})[b]		
F_{NOE}	21.0 ± 3.7	17.6
F_{tor}	0.013 ± 0.056	0.0
F_{repel}	1.24 ± 0.78	0.9
RMS deviations from idealized geometry		
bonds (Å)	0.004 ± 0.0003	0.004
angles (deg)	0.355 ± 0.043	0.333
impropers (deg)	0.300 ± 0.026	0.290
N27A-Aβ (25−35)	16 converged	
RMS deviations from experimental distance constraints (Å)		
all (114)	0.050 ± 0.002	0.044
intraresidue (53)	0.062 ± 0.002	0.058
sequential (32)	0.013 ± 0.007	0.012
medium-range ($\|i - j\| < 5$) (29)	0.048 ± 0.008	0.032
RMS deviation from experimental dihedral constraints (deg) (4)	1.088 ± 0.290	0.59
energetic statistics (kcal mol^{-1})[b]		
F_{NOE}	13.7 ± 1.1	10.5
F_{tor}	0.31 ± 0.15	0.09
F_{repel}	3.78 ± 1.23	3.4
RMS deviations from idealized geometry		
bonds (Å)	0.004 ± 0.0002	0.004
angles (deg)	0.454 ± 0.023	0.420
impropers (deg)	0.403 ± 0.025	0.376

[a] The converged structures refer to the final set of dynamical simulated annealing structures starting from 100 initial random structures; the mean structure was obtained by restrained minimization of the averaged coordinate of the individual structures. The number of each experimental constraint used in the calculations are given in parentheses. [b] F_{NOE}, F_{tor}, and F_{repel} are the energies related to the NOE violations, the torsion angle violations and the van der Waals repulsion term, respectively. The values of the force constants used for these terms are the standard values as depicted in X-PLOR 3.1 manual.

residue and 58 inter-residue NOE distance constraints. In the case of N27A-Aβ (25−35), the input data of the NMR experimental constraints consisted of 114 distance and four dihedral constraints. All 114 distance constraints include 53 intra-residue and 61 inter-residue NOE distance constraints.

Simulated annealing calculations were started from 100 initial random structures for each peptide. We selected 20 and 16 final solution structures with the lowest energy for Aβ (25−35) and N27A-Aβ (25−35), respectively, that were in good agreement with the NMR experimental constraints, for which the NOE distance and torsion angle violation were smaller than 0.5 Å and 5°, respectively. Structural statistics for the mean and converged structures for both Aβ (25−35) and N27A-Aβ (25−35) were evaluated in terms of structural parameters, as shown in Table 2. The convergence was

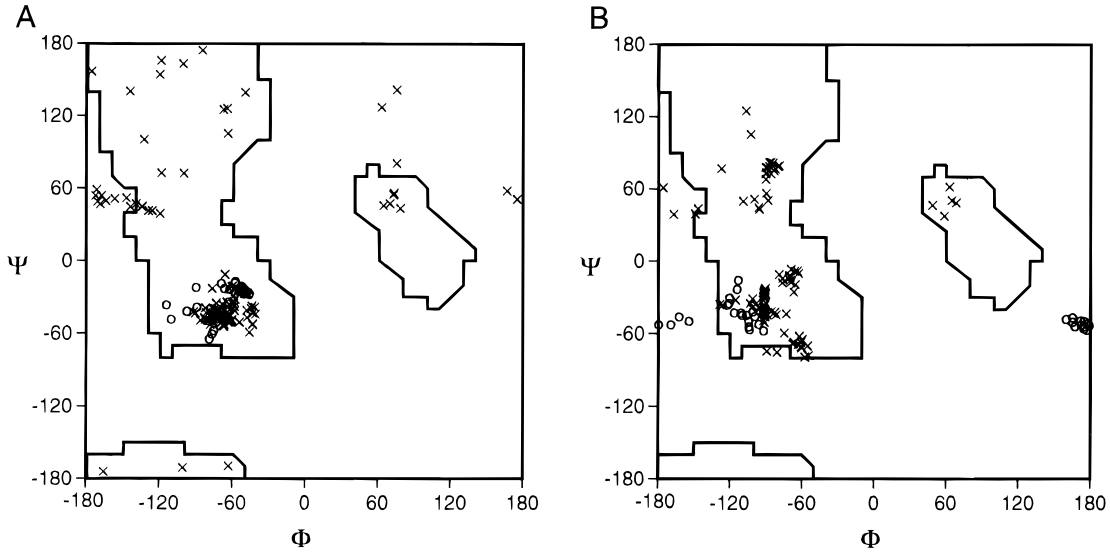

FIGURE 5: Ramachandran plots of the backbone conformational (ϕ, ψ) angles for all residues of the converged structures of Aβ (25−35) (A) and N27A-Aβ (25−35) (B). The circles (○) indicate glycine residues and the crosses (×) indicate other residues.

Table 3: Root Mean Square Differences for the Converged Structures of Aβ (25−35) and N27A-Aβ (25−35)[a]

	atomic RMS differences of converged structures versus mean structure (Å)		average pairwise RMS differences for converged structures (Å)	
	residues 25−35	residues 28−34	residues 25−35	residues 28−34
Aβ (25−35) (20 converged structures)				
backbone				
(N, C$^\alpha$, C)	1.04 ± 0.25	0.26 ± 0.11	1.44 ± 0.53	0.38 ± 0.15
(N, C$^\alpha$, C, O)	1.02 ± 0.23	0.30 ± 0.14	1.42 ± 0.48	0.45 ± 0.19
all heavy atoms	1.39 ± 0.27	0.77 ± 0.21	1.99 ± 0.50	1.11 ± 0.31
N27A-Aβ (25−35) (16 converged structures)				
backbone				
(N, C$^\alpha$, C)	0.49 ± 0.08	0.16 ± 0.08	0.70 ± 0.18	0.24 ± 0.11
(N, C$^\alpha$, C, O)	0.53 ± 0.06	0.20 ± 0.09	0.76 ± 0.18	0.29 ± 0.12
all heavy atoms	1.11 ± 0.13	0.88 ± 0.15	1.60 ± 0.30	1.27 ± 0.33

[a] The RMSD values were obtained by fitting the backbone atoms (N, C$^\alpha$, C, O) coordinates for the residues of the converged structures. The numbers given for the backbone and all heavy atoms represent the mean values ± standard deviations.

further assessed by the (ϕ, ψ) spacing for all selected structures. In a Ramachandran-type plots (Figure 5A,B), the backbone dihedral angles for the all residues of the final converged structures fall either in the α-helical region or in generally allowed regions for both Aβ (25−35) and N27A-Aβ (25−35).

The overall convergence for the final set of structures can be quantified by an atomic RMSD value. In the case of Aβ (25−35), the RMS differences from the averaged coordinate positions were 1.04 ± 0.25 Å for the backbone atoms (N, C$^\alpha$, C) and 1.39 ± 0.27 Å for all heavy atoms. For the same atom selection, the average pairwise RMSD of the 20 individual structures were 1.44 ± 0.53 Å and 1.99 ± 0.50 Å, respectively (Table 3). In the case of N27A−Aβ (25−35), the RMS differences from the averaged coordinate positions were 0.49 ± 0.08 Å for the backbone atoms (N, C$^\alpha$, C) and 1.11 ± 0.13 Å for all heavy atoms. For the same atom selection, the average pairwise RMSD of the 16 individual structures was 0.70 ± 0.18 Å and 1.60 ± 0.30 Å, respectively (Table 3). Both peptides show rather high RMSD values. That would be because N-terminal portion of each peptide is disordered. This explanation is supported by low RMSD value in the C-terminal region of each peptide described below.

Figures 6B and 6C show the distribution of the atomic RMSD for the 20 converged structures of Aβ (25−35) fitted over the backbone heavy atoms (N, C$^\alpha$, C, O) of residues Lys^{28}-Leu^{34} of the mean structure as a function of the residue number. The backbone structure is well defined through Lys^{28}-Leu^{34} of the molecule. This is supported by RMSD values of Lys^{28}-Leu^{34} region. In this region, the RMS differences from the averaged coordinate positions were 0.26 ± 0.11 Å for the backbone atoms (N, C$^\alpha$, C) and 0.77 ± 0.21 Å for all heavy atoms. For the same atom selection, the average pairwise RMSD was 0.38 ± 0.15 Å and 1.11 ± 0.31 Å, respectively (Table 3). However, the portion of N-terminal three residues, Gly^{25} and Ser^{26}, is rather disordered. The disorder in this region corresponds to order parameter S (Figure 6D). Only ψ of Gly^{25}, ϕ and ψ of Ser^{26}, and ϕ of Asn^{27} have lower angular order parameters (S < 0.8) among all the ϕ and ψ angles.

Figures 6F and 6G show the distribution of the atomic RMSD for the 16 converged structures of N27A-Aβ (25−35) fitted over the backbone heavy atoms (N, C$^\alpha$, C, O) of residues Lys^{28}-Leu^{34} of the mean structure as a function of the residue number. The backbone structure is well defined through Ala^{27}-Leu^{34} of the molecule. This is supported by the RMSD values of the Lys^{28}-Leu^{34} region. In this region, the RMS differences from the averaged coordinate positions were 0.16 ± 0.08 Å for the backbone atoms (N, C$^\alpha$, C) and 0.88 ± 0.15 Å for all heavy atoms. For the same atom selection, the average pairwise RMSD was 0.24 ± 0.11 Å

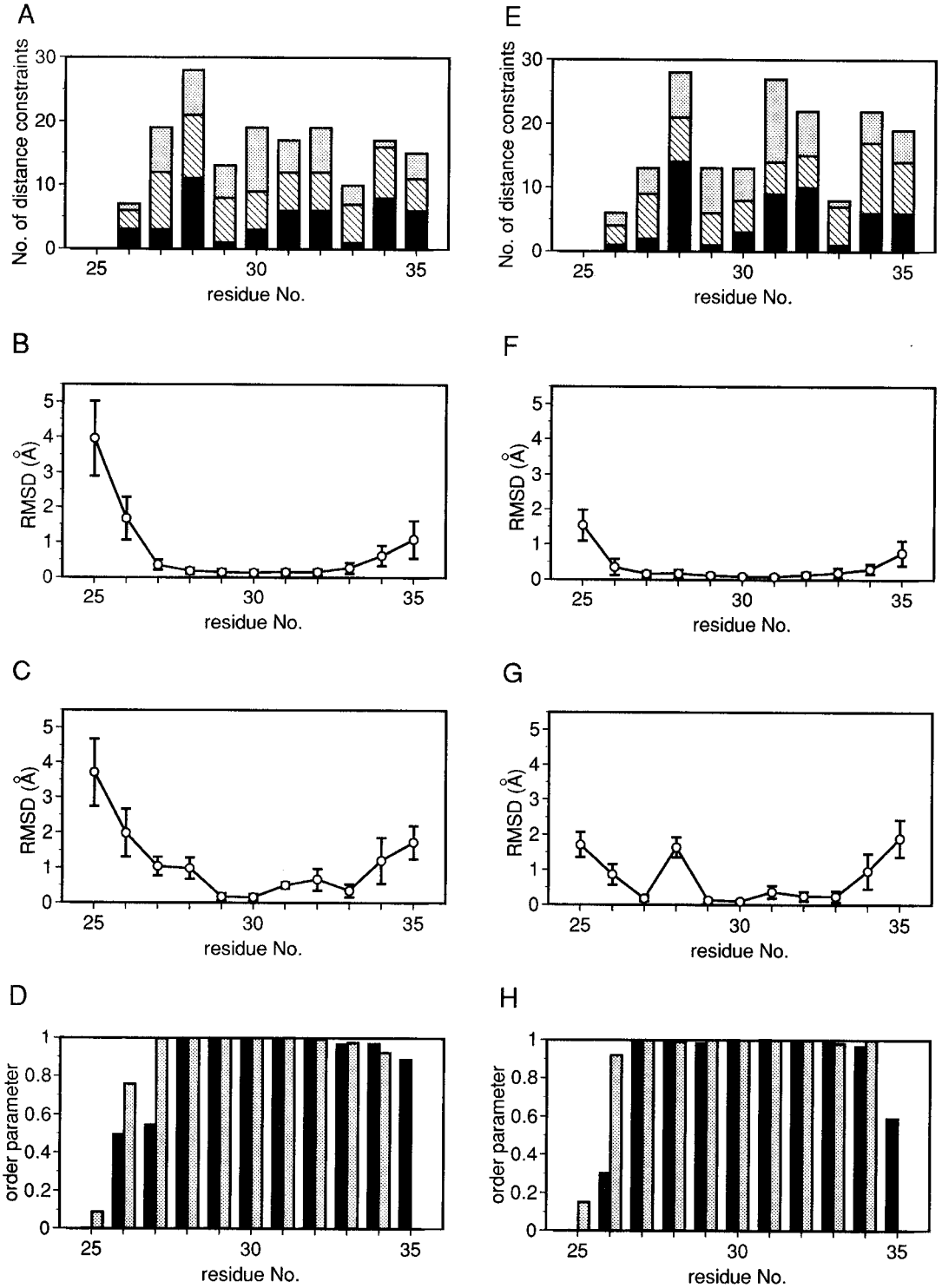

FIGURE 6: Backbone variability by residue of Aβ (25−35) (A−D) and N27A-Aβ (25−35) (E−H), respectively. (A, E) Distribution of the number of experimental distance constraints as a function of the sequence position of Aβ (25−35) and N27A-Aβ (25−35), respectively. Filled bars, intra-residue NOEs; hatched bars, sequential NOEs; stippled bars, medium-range NOEs; open bars, all long-range constraints. (B, C, F, G) Distribution of the RMS distance of the backbone (B and F) and all heavy atoms (C and G) from the mean structure as a function of residue number is shown together with the standard deviations in these values. (D, H) Filled bars, the order parameter S of the ϕ; shaded bars, the order parameter S of the ψ, 0 = randomly distributed, and 1 = perfectly aligned.

and 1.27 ± 0.33 Å, respectively (Table 3). However, a portion of N-terminal two residues, Gly[25] and Ser[26], is rather disordered. In the N-terminal region, only the ψ of Gly[25] and ϕ of Ser[26] have lower angular order parameters (S < 0.8).

Description of the Three-Dimensional Structure. Figures 7A and 7B show stereopair representations of the best-fit superposition of the backbone heavy atoms (N, C^{α}, C) of Lys[28]-Leu[35] for the 20 and 16 converged structures of Aβ (25−35) and N27A-Aβ (25−35), respectively. Analysis of the 20 and 16 converged structures indicates that both the molecular structures of Aβ (25−35) and N27A-Aβ (25−35) contain an α-helical region in the C-terminal part of the sequence. In the case of Aβ (25−35), the extent of α-helix is from Lys[28] to Met[35], which is identified from the Ramachandran plot (Figure 5A) and the order parameters

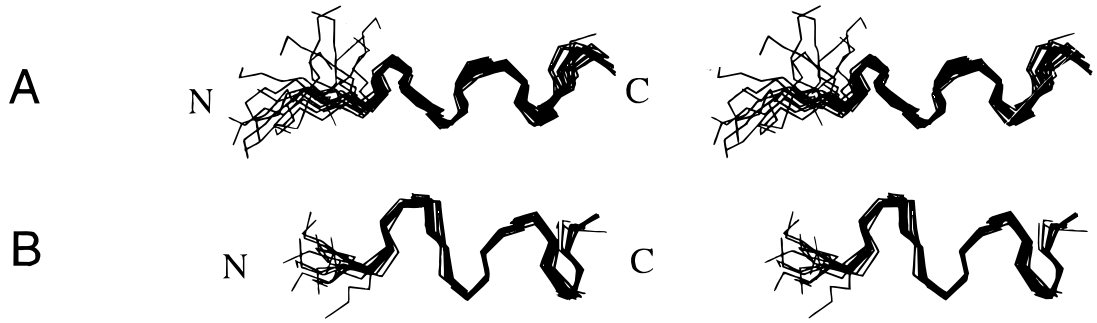

FIGURE 7: Stereopairs of backbone heavy atoms (N, C^{α}, and C) for the 20 and 16 converged structures of Aβ (25−35) (A) and N27A-Aβ (25−35) (B), respectively. These are the results of the best-fit superposition of the backbone heavy atoms (N, C^{α}, C) of Lys^{28}-Leu^{35} shown using MIDAS Plus (Ferrin et al., 1988).

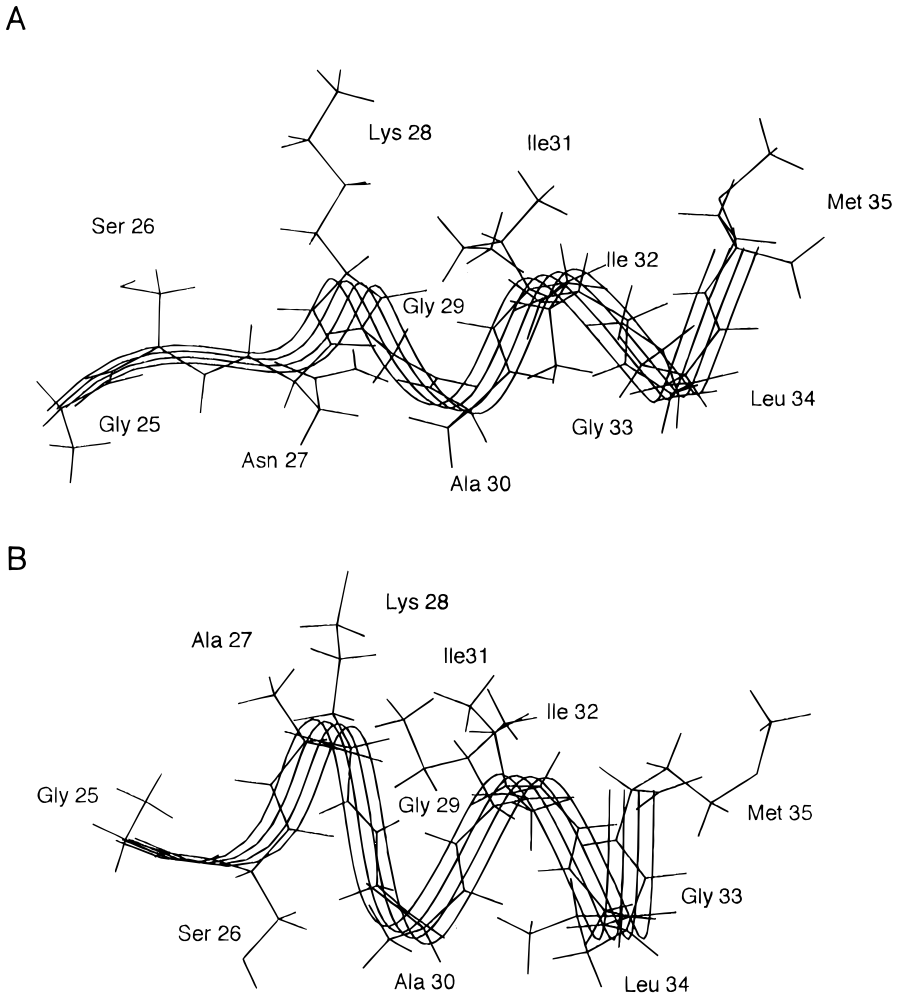

FIGURE 8: Averaged structures with ribbon diagrams of Aβ (25−35) (A) and N27A-Aβ (25−35) (B).

of ϕ and ψ (Figure 6D). In the case of N27A-Aβ (25−35), the extent of α-helix is from Ala^{27} to Met^{35} (Figure 5B and 6H). The N-terminal region of both peptides is disordered; from Gly^{25} to Asn^{27} for Aβ (25−35) and from Gly^{25} to Ser^{26} for N27A-Aβ (25−35). This non-helical region is identified from Figures 8A and 8B in which the averaged structures with ribbon diagrams of Aβ (25−35) and N27A-Aβ (25−35) are shown, respectively.

Temperature Coefficients and NH-Hydrogen Exchange. The temperature dependence of the amide proton chemical shift indicates whether it is protected from exchange with the solvent. For a random-coil peptide in water, the temperature coefficients of the amide proton resonances are expected to be $6 \leq -\Delta\delta/\Delta T \leq 10$ ppb, whereas for amide protected from exchange with the solvent these values are expected to decrease to $-\Delta\delta/\Delta T \leq 5$ ppb (Rose et al., 1985). The temperature coefficients for the amide backbone protons of Aβ (25−35) and N27A-Aβ (25−35) are shown in Table 4. The decreased temperature coefficients of the amides of C-terminal three residues in both Aβ (25−35) and N27A-Aβ (25−35) suggest that these residues would be deeply buried in the micelles. We also determined the time of disappearance of each amide proton resonances after the solvent was exchanged from H_2O to ^2H_2O (Table 4). The results of NH-hydrogen exchange show that the amide protons in the C-terminal region of both β (25−35) and N27A-Aβ (25−35) are protected against the solvent. These data suggest that C-terminal region of both β (25−35) and

Table 4: Temperature Coeffcients and NH-Hydrogen Exchange Time for Aβ (25−35) and N27A-Aβ (25−35)

residue	$-\Delta\delta/\Delta T \times 1000$[a]	h[b]
	(A) Aβ (25−35)	
Gly25	*c*	*c*
Ser26	6.2	0.5
Asn27	3.9	0.5
Lys28	1.4	0.5
Gly29	7.1	0.5
Ala30	4.7	2.0
Ile31	4.6	>8.0
Ile32	6.5	>8.0
Gly33	2.4	5.0
Leu34	3.0	>8.0
Met35	0.4	>8.0
	(B) N27A-Aβ (25−35)	
Gly25	*c*	*c*
Ser26	4.9	0.5
Ala27	6.0	0.5
Lys28	5.8	0.5
Gly29	4.1	2.0
Ala30	3.5	3.5
Ile31	9.6	>8.0
Ile32	5.0	>8.0
Gly33	2.6	5.0
Leu34	2.0	>8.0
Met35	0.8	>8.0

[a] Temperature coefficient values. Uncertainty in the temperature coefficient values is ±0.5 ppb/K. [b] The time when the amide proton resonance disappeared in TOCSY spectrum after the solvent was exchanged. [c] Not detected (N-terminus).

N27A-Aβ (25−35) is deeply buried in the micelles, whereas N-terminal region is exposed to the solvent.

DISCUSSION

Structural Features of Aβ (25−35) in a Membrane-Mimicking Environment. In the present study, we have determined the first high-resolution solution structure of the neurotoxic Aβ (25−35) and its non-neurotoxic mutant [N27A-Aβ (25−35)] in the membrane-mimicking environment by NMR spectroscopy. The previous reports show that Aβ (1−28) adopts an α-helical conformation in a membrane-mimicking environment (Barrow et al., 1992; Barrow & Zagorski, 1991; Talafous et al., 1994). However, this region does not possess neurotoxic activity by itself. Recently, a structural model for the amyloid β fibril comprising Aβ (34−42) was analyzed by ^{13}C solid-state NMR spectroscopy (Lansbury et al., 1995). In this model, the peptide Aβ (34−42) forms an anti-parallel β-sheet structure. Hilbich et al. (1991) proposed that aggregated Aβ (10−42) adopts a β-sheet conformation with a central β-turn from residues Ser^{26} to Gly^{29}. These model suggest the structurural features of Aβ in the amyloid fibril.

Previous work also established that in membrane systems, the amyloid β peptide does not aggregate, but produces voltage-dependent ion channels (Arispe et al., 1993a,b). Theoretical models of the possible ion channel structure of amyloid β-peptide have also been reported (Durell et al., 1994).

Very recently, Sticht et al. (1995) reported a tertiary structure of Aβ (1−40) in a 40% mixture of deuterated 2,2,2-trifluoroethanol (TFE) and water, in which two helices, Gln^{15}-Asp^{23} and Ile^{31}-Met^{35}, were found as main secondary-structure elements. However, SDS micelles are a more suitable model for the essentially anisotropic native membrane environment than the mixture of water and organic solvent such as TFE is (Pervushin & Arseniev, 1992). Moreover, Aβ (25−35) in LiDS micelles is very stable; it did not aggregate for at least several months, whereas Sticht et al. (1995) reported that Aβ (1−40) in a 40% mixture of deuterated TFE and water was stable only for 3 days. In this study, we used LiDS micelles instead of SDS micelles, because LiDS is more soluble than SDS is, especially at low temperature (Henry & Sykes, 1994). Therefore, our structure probably shows a more likely model for Aβ in the biological membrane.

The structure of Aβ (25−35) in the LiDS micelles which we have shown in this study consists of an α-helix in the C-terminal region and a disordered stretch in the N-terminal region. This structure in micelles is different from those in aggregated form previously reported (Hilbich et al., 1991; Lansbury et al., 1995). As for the amino acid sequence, the four amino acid residues from the N-terminus are rather hydrophilic and the other seven amino acid residues in C-terminus are rather hydrophobic. From the amino acid sequences and temperature coefficients of amide proton chemical shifts, it is suggested that the C-terminal region of Aβ (25−35) is buried in the membrane and assumes α-helical structure, whereas the N-terminal region is exposed to the solvent with a flexible structure. The structure and function relationships of Aβ (25−35) will be discussed later.

Aβ (25−35) and Ion Channels. So far, many hypotheses have been proposed to explain the neurotoxicity induced by Aβ. Previous work reported that Aβ forms voltage-dependent ion channels (Arispe et al., 1993a,b). Theoretical models of the possible ion channel structure of amyloid β-peptide are also reported (Durell et al., 1994). From the NMR study of Aβ (1−28) in TFE solvent, Talafous (1994) showed the similarity between the structure of Aβ (1−28) and that of alamethicin (Fox & Richards, 1982) and melittin (Terwilliger & Eisenberg, 1982) and proposed that the Aβ ion channel consists of a tetrameric α-helical structure. Furukawa et al. (1994) speculated that the pores in the cell membrane are made by Aβ (25−35). In the case of Aβ (25−35), however, the three-dimensional structure in the micelles determined in this study consists of α-helix with extended N-terminal region. To span the native lipid bilayer as an α-helix, at least twenty amino acid residues are needed (Henry & Sykes, 1994). Therefore, it is seems to be impossible for Aβ (25−35) to form an ion channel in the native lipid bilayer. Another mechanism should be considered to explain the neurotoxicity caused by Aβ (25−35).

Comparison of the Structures of Aβ (25−35) and N27A-Aβ (25−35). In the present study, we have not only determined the structure of Aβ (25−35) but also that of N27A-Aβ (25−35), which is a non-neurotoxic mutant, as shown in our previous report (Sato et al., 1995). In this mutant, a hydrophilic residue, Asn^{27}, is replaced by a hydrophobic residue, Ala. We suspected that this mutant might show higher hydrophobicity and more toxicity due to increased hydrophobicity. But it was less potent than Aβ (25−35). Therefore, it is important to compare the structures of Aβ (25−35) and N27A-Aβ (25−35) to understand the mechanism of neurotoxicity of Aβ.

Here, we have elucidated the both structures of Aβ (25−35) and N27A-Aβ (25−35) in LiDS micelles. Both structures possess an α-helix in the C-terminal region, but the structure of N-terminal region of the peptides is slightly

different from each other. In the case of Aβ (25−35), N-terminal region are more flexible than that of N27A-Aβ (25−35). In LiDS micelles, the hydrophilic N-terminal region of Aβ (25−35) is assumed to expose to solvent, whereas hydrophobic C-terminal region is assumed to be buried in the micelles. So the difference of the structure of the N-terminal region of Aβ (25−35) and N27A-Aβ (25−35) may correspond to the difference of the condition of solvent-exposed region of Aβ peptides.

Comparison of the Structures of Aβ (25−35) and Substance P. Recently, we showed that Aβ (25−35) inactivates phosphatidyl inositol-3 kinase in hippocampal culture (Takashima et al., 1996), which suggests the possibility that Aβ (25−35) exerts its activity by interacting with cell surface receptors. In this regard, it is important to interpret the tertiary structure of Aβ bound within the membrane, which is possibly an active conformation for interaction with a receptor. Formerly, it was reported that Aβ function as a peptide ligand of substance P receptors with some pathophysiologic activities (Shimohigashi et al., 1993). Another work reported that Aβ is recognized by the separin−enzyme complex receptor in hepatoma cells and neuronal cells (Boland et al., 1995). Sequence similarity between Aβ (25−35) and substance P was first noticed by Yankner et al. (1990) (Figure 1). Shimohigashi et al. (1993) have shown that Aβ (21−35)-NH_2 is a highly selective agonist of substance P receptors (NK-1) among three tachykinin receptor subtypes. The three mammalian tachykinins or neurokinins—substance P, neurokinin A, and neurokinin B—are reported to bind selectively to three distinct tachykinin receptor subtype, NK-1, NK-2, and NK-3, sites, respectively (Buck & Burcher, 1986; Laufer et al., 1986; Regoli et al., 1987). The membrane-mediated structure of substance P was predicted by Schwyzer et al. (1986). In this prediction, the C-terminal message-containing nonapeptide segment of substance P is almost perpendicularly oriented to the membrane in the α-helical domain, whereas the N-terminal segment remains in the aqueous phase as a random-coil domain. Such a conformation of substance P in the membrane was confirmed using CD (Rolka et al., 1986) and IR (Erne et al., 1986). Young et al. (1994) reported the three-dimensional structure of substance P in the presence of 15 mM SDS micelles determined by using NMR. This structure corresponds to the predicted structure. The NMR structure of substance P consists of an N-terminal flexible region of three residues and a C-terminal helical region. In the case of substance P, the membrane-mediated structure is essential for the binding to its specific receptors (Schwyzer, 1987). The structure of Aβ (25−35) in LiDS micelles shown in the present study (Figure 8) is very similar to this membrane-mediated structure of substance P. The structure of Aβ (25−35) consists of an N-terminal flexible region of three residues and a C-terminal helical region. This similarity gives the structural evidence that Aβ (25−35) interacts with a membrane protein such as a substance P receptor in a same manner as substance P.

Structure-Function Relationships of Aβ. Our previous report shows that N27A-Aβ (25−35) where Asn^{27} is replaced by Ala shows lower neurotoxicity than wild type despite of its increase of hydrophobicity (Sato et al., 1995). The results of sedimentation measurements indicate that N27A-Aβ (25−35) has the tendency not to aggregate (Sato et al., 1995).

One explanation for the relationship between the aggregation tendency of each Aβ (25−35) mutant and its neurotoxicity is as follows. Aβ (25−35) shows neurotoxicity when it binds to the membrane and assumes the appropriate structure similar to the membrane-mediated structure of substance P. And an intermediate between monomer and highly-aggregated form may have a high affinity for the membrane. So the correlation between the aggregation and neurotoxicity may be attributed to the correlation between the contents of intermediates and neurotoxicity. In this regard, it may be that N27A-Aβ (25−35) has weak neurotoxic activity because this mutant has a lower tendency to form aggregate intermediates needed for binding to the membrane.

Another reason why N27A-Aβ (25−35) has weak neurotoxic activity may be explained from the comparison of the membrane-mediated structures of Aβ (25−35), N27A-Aβ (25−35), and substance P. In the last section we have shown that Aβ (25−35) assumes a membrane-mediated structure very similar to that of substance P. Both structures consist of N-terminal flexible region exposed to the solvent and C-terminal helical region buried in the membrane. In the case of N27A-Aβ (25−35), the membrane-mediated structure is rather different from the structures of Aβ (25−35) and substance P. It has a C-terminal helical region, but its N-terminal region is more rigid and not so extended compared with those of Aβ (25−35) and substance P. This suggests that N27A-Aβ (25−35) is buried in the membrane in a manner different from that of Aβ (25−35) or substance P. In N27A-Aβ (25−35), a hydrophilic residue, Asn^{27}, is replaced by a hydrophobic residue, Ala. N27A-Aβ (25−35) may be more deeply buried in the membrane than Aβ (25−35) and substance P. This difference may cause a reduced or loss of the activity of N27A-Aβ (25−35) for binding to the specific membrane protein, like the substance P receptor.

In conclusion, we have determined the membrane-mediated structures of Aβ (25−35) and N27A-Aβ (25−35). The structure of Aβ (25−35) consists of N-terminal flexible region and C-terminal helical region and is very similar to that of substance P whereas that of N27A-Aβ (25−35) is rather different. This comparison gives a structural basis to understand the mechanism of neurotoxicity caused by Aβ.

ACKNOWLEDGMENT

We thank Miss Akiko Wakamiya for the synthesis of both Aβ (25−35) and N27A-Aβ (25−35). We also thank Dr. Kaori Wakamatsu for the preparation of lithium dodecyl sulfate and helpful discussion. We also thank Drs. Katsuo Katayanagi, Takao Matsuzaki, and Yoshio Kodera for helpful discussions. We also thank Dr. Arno Pähler for critical reading of this manuscript.

REFERENCES

Arispe, N., Pollard, H. B., & Rojas, E. (1993a) *Proc. Natl. Acad. Sci. U.S.A. 90*, 10573−10577.
Arispe, N., Rojas, E., & Pollard, H. B. (1993b) *Proc. Natl. Acad. Sci. U.S.A. 90*, 567−571.
Barrow, C. J., & Zagorski, M. G. (1991) *Science 253*, 179−182.
Barrow, C. J., Yasuda, A., Kenny, P. T. M., & Zagorski, M. G. (1992) *J. Mol. Biol. 225*, 1075−1093.
Bax, A., & Davis, D. G. (1985) *J. Magn. Reson. 65*, 355−359.
Boland, K., Manias, K., & Perlmutter, D. H. (1995) *J. Biol. Chem. 270*, 28022−28028.

Brünger, A. T. (1993) *X-PLOR Manual, Version 3.1*, Yale University, New Haven, CT.
Buck, S. H., & Burcher, E. (1986) *Trends. Pharmacol. Sci. 7*, 65−68.
Busciglio, J., Lorenzo, A., & Yankner, B. A. (1993) *J. Neurochem. 61*, 1565−1568.
Clore, G. M., Gronenborn, A. M., Nilges, M., & Ryan, C. A. (1987) *Biochemistry 26*, 8012−8023.
Davis, J. H., Bradley, E. K., Miljanich, G. P., Nadasdi, L., Ramachandran, J., & Basus, V. J. (1993) *Biochemistry 32*, 7396−7405.
Durell, S. R., Guy, H. R., Arispe, N., Rojas, E., & Pollard, H. B. (1994) *Biophys. J. 67*, 2137−2145.
Erne, D., Rolka, K., & Schwyzer, R. (1986) *Helv. Chim. Acta 69*, 1807−1816.
Ferrin, T. E., Huang, C. C., Jarvis, L. E., & Langridge, R. (1988) *J. Mol. Graphics 6*, 13−27.
Fox, R. O., & Richards, F. M. (1982) *Nature 300*, 325−330.
Furukawa, K., Abe, Y., & Akaike, N. (1994) *NueroReport 5*, 2016−2018.
Hardy, J. A., & Higgins, G. A. (1992) *Science 256*, 184−185.
Henry, G. D., & Sykes, B. D. (1994) *Methods Enzymol. 239*, 515−535.
Hilbich, C., Woike, B. K., Reed, J., Masters, C. L., & Beyreuther, K. (1991) *J. Mol. Biol. 218*, 149−163.
Hurd, R. E. (1990) *J. Magn. Reson. 87*, 422−428.
Hyberts, S. G., Goldberg, M. S., Havel, T. F., & Wagner, G. (1992) *Protein Sci. 1*, 736−751.
Jeener, J., Meier, B. H., Bachmann, P., & Ernst, R. R. (1979) *J. Chem. Phys. 71*, 4546−4553.
Kirschner, D. A., Inoue, H., Duffy, L. K., Sinclair, A., Lind, M., & Selkoe, D. J. (1987) *Proc. Natl. Acad. Sci. U.S.A. 1987*, 6953−6957.
Koh, J.-Y., Yang, L. L., & Cotman, C. W. (1990) *Brain Res. 533*, 315−320.
Lansbury, P. T., Jr., Costa, P. R., Griffiths, J. M., Simon, E. J., Auger, M., Halverson, K. J., Kocisko, D. A., Hendsch, Z. S., Ashburn, T. T., Spencer, R. G. S., Tidor, B., & Griffin, R. G. (1995) *Nat. Struct. Biol. 2*, 990−998.
Laufer, R., Gilon, C., Chorev, M., & Selinger, Z. (1986) *J. Biol. Chem. 261*, 10257−10263.
Macura, S., Huang, Y., Suter, D., & Ernst, R. R. (1981) *J. Magn. Reson. 43*, 259−281.
Marion, D., & Wüthrich, K. (1983) *Biochem. Biophys. Res. Commun. 113*, 967−974.
Mattson, M. P., Cheng, B., Davis, D., Bryant, K., Lieberburg, I., & Rydel, R., E. (1992) *J. Neurosci. 12*, 376−389.
Mattson, M. P., Tomaselli, K. J., & Rydel, R. E. (1993) *Brain Res. 621*, 35−49.
Pardi, A., Billerter, M., & Wüthrich, K. (1984) *J. Mol. Biol. 180*, 741−751.
Pervushin, K. V., & Arseniev, A. S. (1992) *FEBS Lett. 308*, 190−196.
Pike, C. J., Burdick, D., Walencewicz, A. J., Glabe, C. G., & Cotman, C. W. (1993) *J. Neurosci. 13*, 1676−1687.
Piotto, M., Saudek, V., & Sklenár, V. (1992) *J. Biomol. NMR 2*, 661−665.
Ramachandran, G. N., Ramakrishnan, C., & Sasisekharan, V. (1963) *J. Mol. Biol. 7*, 95−99.
Rance, M., Sørensen, O. W., Bodenhausen, G., Wagner, G., Ernst, R. R., & Wüthrich, K. (1983) *Biochem. Biophys. Res. Commun. 117*, 479.
Regoli, D., Drapeau, G., Dion, S., & D'Orléans-Juste, P. (1987) *Life Sci. 40*, 109−117.
Rolka, K., Erne, D., & Schwyzer, R. (1986) *Helv. Chim. Acta 69*, 1798−1806.
Rose, G. D., Gierasch, L. M., & Smith, J. A. (1985) *Adv. Protein Chem. 37*, 1−109.
Sato, K., Wakamiya, A., Maeda, T., Noguchi, K., Takashima, A., & Imahori, K. (1995) *J. Biochem. 118*, 1108−1111.
Schwyzer, R. (1987) *EMBO J. 6*, 2255−2259.
Schwyzer, R., Erne, D., & Rolka, K. (1986) *Helv. Chim. Acta 69*, 1789−1797.
Shimohigashi, Y., Matsumoto, H., Takano, Y., Saito, R., Iwata, T., Kamiya, H., & Ohno, M. (1993) *Biochem. Biophys. Res. Commun. 193*, 624−630.
Sklenár, V., Piotto, M., Leppik, R., & Saudek, V. (1993) *J. Magn. Reson. Ser. A 102*, 241−245.
Spera, S., & Bax, A. (1991) *J. Am. Chem. Soc. 113*, 5490−5492.
Sticht, H., Bayer, P., Willbold, D., Dames, S., Hilbich, C., Beyreuther, K., Frank, R. W., & Rösch, P. (1995) *Eur. J. Biochem. 233*, 293−298.
Takashima, A., Noguchi, K., Sato, K., Hoshino, T., & Imahori, K. (1993) *Proc. Natl. Acad. Sci. U.S.A. 90*, 7789−7793.
Takashima, A., Noguchi, K., Michel, G., Mercken, M., Hoshi, M., Ishiguro, K., & Imahori, K. (1996) *Neurosci. Lett. 203*, 33−36.
Talafous, J., Marcinowski, K. J., Klopman, G., & Zagorski, M. G. (1994) *Biochemistry 33*, 7788−7796.
Terwilliger, T. C., & Eisenberg, D. S. (1982) *J. Biol. Chem. 257*.
Tomiyama, A., Asano, S., Suwa, Y., Morita, T., Kataoka, K.-I., Mori, H., & Endo, N. (1994) *Biochem. Biophys. Res. Commun. 204*, 76−83.
von Kienlin, M., Moonen, C. T. W., van der Toorn, A., & van Zijl, P. C. M. (1991) *J. Magn. Reson. 93*, 423−429.
Wishart, D. S., & Sykes, B. D. (1994) *Methods Enzymol. 239*, 363−392.
Wishart, D. S., Sykes, B. D., & Richards, F. M. (1992) *Biochemistry 31*, 1647−1651.
Wüthrich, K. (1986) *NMR of Proteins and Nucleic Acids*, Wiley, New York.
Wüthrich, K., Billeter, M., & Braun, W. (1983) *J. Mol. Biol. 169*, 949−961.
Wüthrich, K., Billeter, M., & Braun, W. (1984) *J. Mol. Biol. 180*, 715−740.
Yankner, B. A., Duffy, L. K., & Kirschner, D. A. (1990) *Science 250*, 279−282.
Young, J. K., Anklin, C., & Hicks, R. P. (1994) *Biopolymers 34*, 1449−1462.

BI961598J